Applied Physics Letters

Effect of gas mixture on temperature and mass streaming in a phase-change thermoacoustic engine

Cite as: Appl. Phys. Lett. **116**, 243701 (2020); https://doi.org/10.1063/5.0009599
Submitted: 01 April 2020 . Accepted: 30 May 2020 . Published Online: 16 June 2020

Tom Brustin, Avshalom Offner, and Guy Z. Ramon

AIP Publishing

Applied Physics Letters ARTICLE scitation.org/journal/apl

Effect of gas mixture on temperature and mass streaming in a phase-change thermoacoustic engine

Cite as: Appl. Phys. Lett. **116**, 243701 (2020); doi: 10.1063/5.0009599
Submitted: 1 April 2020 · Accepted: 30 May 2020 ·
Published Online: 16 June 2020

Tom Brustin, Avshalom Offner, and Guy Z. Ramon[a)]

AFFILIATIONS

Department of Civil and Environmental Engineering and The Nancy and Stephen Grand Technion Energy Program, Technion-Israel Institute of Technology, Haifa 32000, Israel

[a)]Author to whom correspondence should be addressed: ramong@technion.ac.il

ABSTRACT

Wet thermoacoustic engines (WTEs) are simple, robust energy conversion devices that employ a condensable vapor to generate acoustic power from heat. While previous studies focused on the potential of WTE technology to convert low-grade heat to power, this work focuses on the WTE's dependence on the working gas mixture, unique mass transport, and low working temperature properties, which make it a potential candidate for thermally driven separation processes, e.g., distillation and water desalination. In a set of experiments, the steady-state behavior of a water-based, standing-wave WTE was studied. The results highlight a remarkable trait of this system—a WTE is capable of producing a substantial flux of water vapor while exhibiting an operating hot-side temperature significantly lower than the boiling point. This "limiting temperature" is independent of the heat input to the system—theoretically predicted in systems that have no external "load" that consumes the acoustic power. In addition, the results suggest that the characteristics of the working gas play an important role in determining the device behavior. It was shown that in the tested range, a heavier, more complex-structured gas has significantly improved the steady-state performance of the engine. Specifically, a WTE working with SF_6 as its working gas exhibited a vapor mass flux nearly three times greater than simple evaporation at the same heating power while maintaining a temperature as low as 57 °C. The link between gas characteristics and engine behavior is outlined. In conclusion, potential applications of the device and future research avenues are discussed.

Low temperature heat obtained, for example, from industrial waste streams, solar irradiation, and geo-thermal, represents a vast, underutilized source of energy.[1] Low-grade heat harvesting solutions include electricity production via organic Rankine and Kalina cycle generators, residential uses such as space and water heating, and industrial thermal processes such as paper production.[1–3] In order to be cost-effective, these technologies must be simple and efficient due to the dispersed nature and, often, low power density of such sources. In particular, low temperature means an inherently low efficiency, which evidently poses a great challenge in making such technologies viable.

Thermoacoustic engines are devices that convert heat into mechanical work in the form of a sound field or vice versa.[4] A unique feature of thermoacoustic (TA) engines is their potential for operation with no moving parts, as the acoustic field may be viewed as a "virtual piston." In such a device, heat is converted into acoustic power due to properly phased heat transfer between a solid and fluid, driven by the interaction between velocity, pressure, and temperature oscillations. In particular, these oscillations may be triggered by generating a temperature difference greater than a threshold value, a state referred to herein as *onset*.

Recent work has demonstrated the promising potential of introducing phase change through an evaporation/condensation or reversible sorption process,[5–9] which we also refer to here as a "wet" thermoacoustic engine, first proposed by Raspet *et al.*[10] In a *wet* thermoacoustic engine (WTE), the working fluid is a mixture of an "inert" gas and a condensable vapor (which we refer to as "reactive," in the broader context, i.e., a reversible sorption reaction). One of the most significant advantages of a WTE is its low onset temperature, which makes it a promising candidate for low-grade heat utilization.

The working cycle of a WTE consists of evaporation occurring during the compression stage of the acoustic cycle, during which mass and associated latent heat are transferred to the gas mixture from the solid boundary which also carries the liquid phase. This is followed by

motion and expansion, during which condensation occurs and the latent heat is transferred to the boundary [see the sketch in Fig. 1(c)]. Due to the added phase change, heat transfer is significantly enhanced, and a time-averaged mass flux is generated in the system—the WTE "pumps" vapor from the hot to the cold end of the stack.

Here, we wish to explore the effect of the inert gas on the onset and limit-cycle characteristics of the WTE and, in particular, the generated mass flux of the condensable species (water, in our case).

The time-averaged axial mass flux in a WTE is given by[5]

$$\dot{m} = \frac{1}{2}\rho_m \Re[\langle \tilde{u}_1 C_1 \rangle] - \rho_m D \frac{dC_m}{dx}, \quad (1)$$

in which ρ_m is the mean density of the mixture, u is the velocity, C is the mass fraction of the reactive species in the mixture, and D is the diffusion coefficient. The subscripts "m" and "1" refer to time-averaged (mean) and oscillating quantities, respectively, angle brackets denote the cross-sectional average, $\Re$ denotes the real part of a complex quantity, and the tilde denotes the complex conjugate. The heat flux consists of a conduction-mediated streaming term and, more importantly, the latent heat carried by the mass streaming,

$$\dot{Q} = \rho_m c_p \Re[\langle \tilde{u}_1 T_1 \rangle] - k\frac{dT_m}{dx} + \dot{m} l_h. \quad (2)$$

Here, c_p is the isobaric heat capacity, T is the temperature, and l_h is the latent heat.

The system transport properties are a function of the working gas characteristics. According to the kinetic theory of gases, the general expressions for the molecular diffusion, dynamic viscosity, and thermal conductivity are[11] $D \propto \frac{T^{3/2}}{pM^{1/2}\sigma^2}$, $\eta \propto \frac{T^{1/2}M^{1/2}}{\sigma^2}$, and $k \propto \frac{T^{1/2}}{M^{1/2}\sigma^2}$, respectively, demonstrating that the transport coefficients are a function of the molar mass, M, and molecular hard-sphere diameter, σ. Hence, to form an experimental set with a wide range of transport properties, we selected three working-gas candidates, ordered from "small/light" to "big/heavy"—argon, CO_2, and SF_6.

The experimental system used herein is sketched in Fig. 1. It consists of a resonator, a "stack" (a cylindrical piece of a ceramic honeycomb), and heat exchangers, which supply and remove heat at the hot and cold sides of the stack, respectively. The stack has 600 channels per square-inch (~1 mm channel height), aligned with the longitudinal axis of the resonator. The hot heat exchanger (HHX) is a corrugated metal strip rolled into a spiral. Heat is provided through two electrical cartridge heaters, whose power supply is adjusted through a pc-controlled user interface. The cold heat exchanger (CHX) is made of three metal pipes, intertwined with copper wire, inserted laterally through the resonator. Cooling water at 20 °C is circulated through the CHX (see the supplementary material for a sketch of the heat exchanger assembly). A pressure sensor is installed at the "hot" end of the resonator, providing pressure measurements from which the pressure amplitude and the resonant frequency are calculated. Three

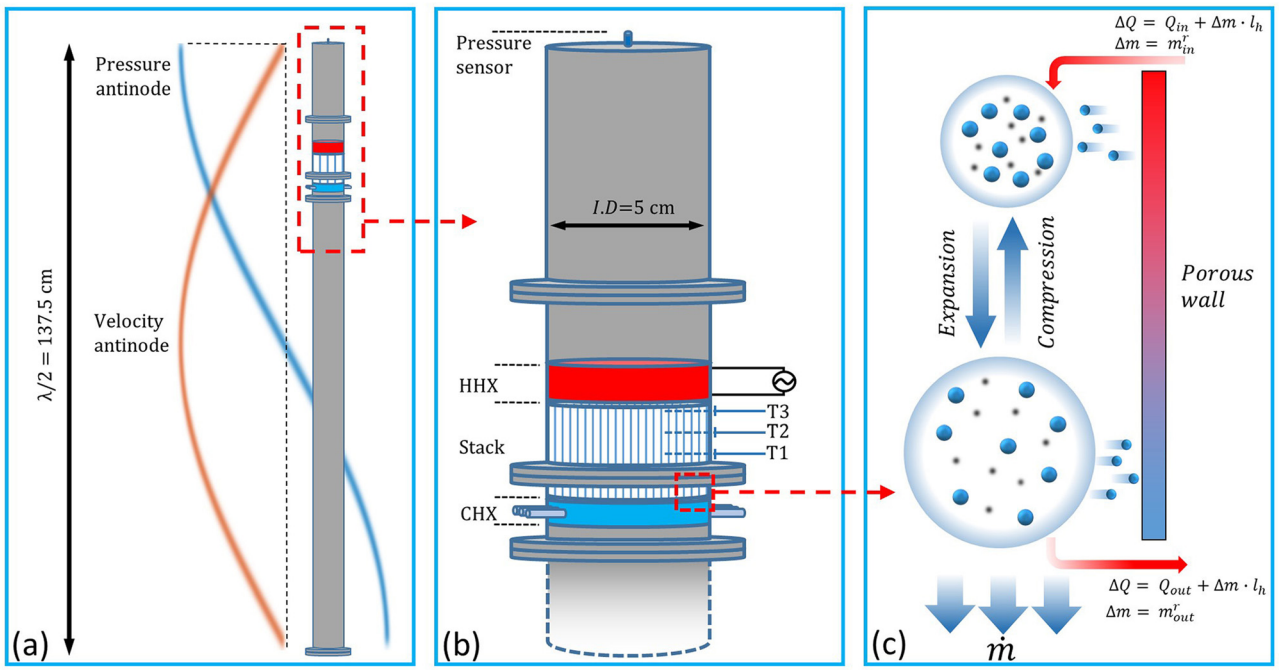

FIG. 1. Schematic depiction of the experimental system design and the thermodynamic cycle of a wet thermoacoustic engine (WTE). (a) The engine body is a stainless steel cylindrical resonator. The resonator is closed on both ends, corresponding to a half-wavelength device. (b) Engine "core": a ceramic honeycomb stack is located between a resistive, hot heat-exchanger (HHX), and a water-cooled cold heat exchanger (CHX), with temperature sensors placed within the stack at 5 mm (T3), 15 mm (T2), and 25 mm (T1) from the stack hot end. A pressure sensor is installed at the resonator end, corresponding to the pressure antinode. (c) Processes undergone by a fluid "parcel" in a wet thermoacoustic work cycle: heat is absorbed via conduction from the solid wall at the hot end, as well as vapor mass of the reactive component (m_r) and its associated latent heat ($m \cdot l_h$). At the cold end, heat is transferred via conduction and mass is rejected due to condensation. The addition of a reactive component (water) results in enhanced heat transport, and a mass transport mechanism is added to the system—vapor mass in a WTE is "pumped" from the hot to the cold side.

temperature sensors (type K thermocouples) are installed along the stack, positioned at 5 mm (T3), 15 mm (T2), and 25 mm (T1) from the hot end. Water, the phase-changing component, was introduced into the system by soaking the porous stack in distilled water prior to each experiment. In order to remove air and introduce the working gas into the system, the resonator was flushed with the designated gas (see the supplementary material for more details of this procedure). Our measurements show that the amount of water lost from the stack due to the flushing process accounts for <3% of the total transported mass, Δm.

Previous work reported a significant challenge in maintaining a steady limit cycle experimentally, primarily due to the partial drying of the stack, as the liquid was evaporated and transported away.[7] Hence, the experimental protocol used in this study was designed such that at least 1000 s of steady state are reached in every given experiment, during which the stack remains wet. A "steady state" (limit cycle) is experimentally defined as a period during which both the pressure amplitude and the temperature profile do not deviate significantly from a stable value. This was achieved by preheating the device at high power until onset is reached and then lowering it to its steady state value (see the supplementary material for the time evolution of a sample experiment). In order to facilitate the measurement of the time-averaged mass transfer, the resonator is placed with the cold side down, such that water condensing on the cold heat exchanger would drip downward, away from the stack. Preliminary experiments showed that the resonator orientation has little effect on the target parameters, an observation that agrees with previous work in the field.[12] Mass transport measurements were obtained by weighing the stack before and after each experiment.

A representative experiment is displayed in Fig. 2, showing the time evolution of the temperature, measured near the hot-end of the stack, for two cases: with and without thermoacoustic oscillations. Both experiments are identical except that in the "no-acoustic" experiment, an obstruction is placed in the resonator (away from the stack), dampening the onset of oscillations. As can be seen, there is a striking difference between the two cases. In both cases, there is an initial steep rise as heating is applied. However, whereas in the absence of the acoustic field, the temperature continuously increases, albeit at a slower rate; throughout the remainder of the experiment, the temperature in the presence of acoustics tapers off and remains constant. Furthermore, this constant temperature varies with the choice of working fluid—it is lower for SF_6 ($57.8 \pm 0.5\,^{\circ}C$), compared to the temperature measured for Ar ($66.5 \pm 0.5\,^{\circ}C$).

Furthermore, the "limiting" temperature reached by the thermoacoustic engine is insensitive to the heating power—it cannot be elevated by increased heating. Apparently, once this temperature is reached, increasing the heating power merely results in more evaporation of water, while the temperature remains unchanged. In the "damped" case, where no acoustic field is present, the temperature continuously rises and will reach the boiling point, given sufficient time. The results indicate that the thermoacoustic field imposes a constraint on the maximal temperature of the liquid at the hot side of the stack, significantly lowering it compared to the saturation point for a given pressure, a phenomenon that represents a unique trait of thermoacoustic action, in both dry and wet systems. This has been previously shown for a dry system[4] and theoretically by Offner *et al.*[13] for a wet system, which is here confirmed experimentally (see the supplementary material for an experiment demonstrating this effect). This characteristic is a consequence of the system configuration, which has no external load consuming power from it. In the presence of a load, the operating temperature will vary. Nevertheless, when the motivation is to generate an evaporative mass flux, such as in a distillation system, there is no power extraction, and therefore, the low operating temperature is potentially advantageous. In this context, another notable difference observed in these experiments is the vapor mass transport. Despite the lower temperatures in the thermoacoustic case, the rate of evaporation was significantly higher compared to the damped case. Specifically, for SF_6, the rate of evaporation was nearly three times higher than that for Ar. Additional results of the mass transport can be found in the supplementary material.

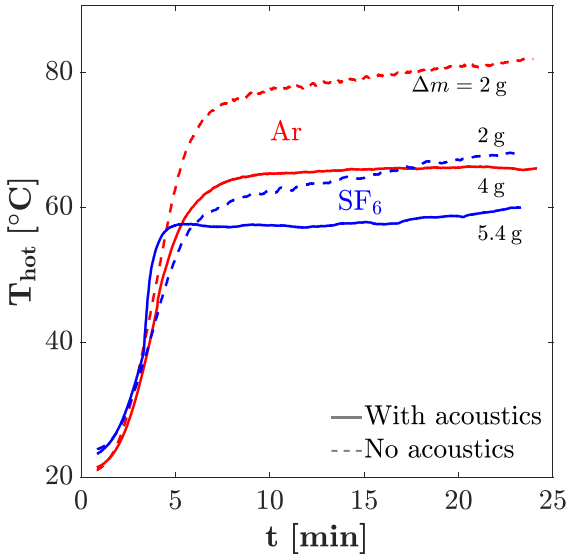

FIG. 2. Representative experimental measurement of the stack hot side temperature for argon (red) and SF_6 (blue) under steady-state operation at 1 bar. Solid lines represent the normal thermoacoustic (TA) operation, while dashed lines represent the damped conditions, i.e., no acoustic field is present. Without the acoustics, heat is transferred primarily through conduction and the experimental duration is too short for the temperature to reach a steady value. Under TA operation, T_{hot} reaches the steady state shortly following onset and saturates at a maximum temperature significantly lower than the boiling point. Mass measurements are indicated next to their respective curves, suggesting that while temperatures are lower, mass transport is significantly enhanced by the acoustic field.

The steady-state temperature profiles along the stack, measured during experiments with different mixtures and at different mean pressures, are shown in Fig. 3. The values plotted in Fig. 3(a) represent the maximum temperature in a given mixture, under thermoacoustic oscillations. The comparison with the saturation temperature illustrates the deviation of each mixture from the boiling point. As discussed earlier, this limiting temperature is lower for the heavier gas. We note that the results for argon at 3 bars are not presented since thermoacoustic oscillations could not be maintained under the supplied heating power, at this pressure. The remaining panels in Fig. 3 present the temperature profile along the stack, at steady state, compared to numerical calculations based on the model developed by Offner *et al.*[13] (see the supplementary material for details of the model). These plots reveal a good quantitative agreement between the

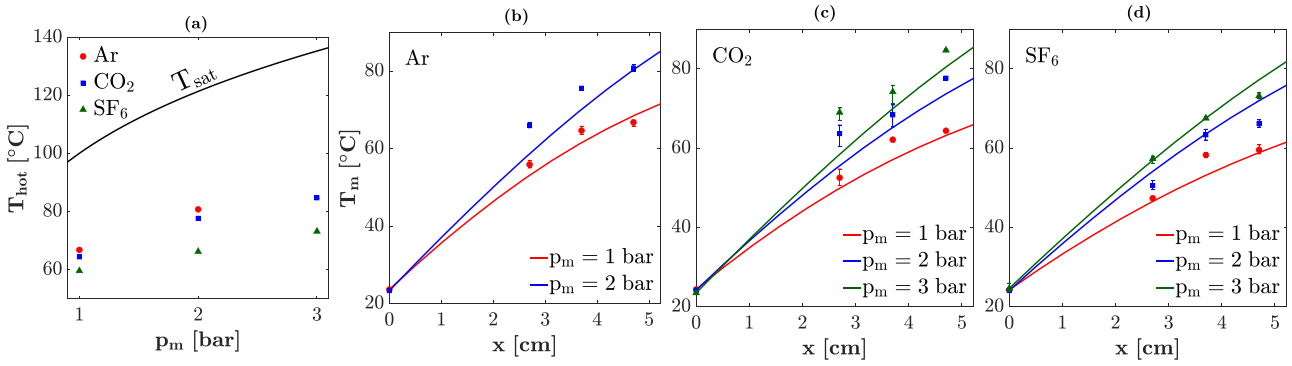

FIG. 3. (a) Hot-side temperature data for three different mixtures and varying mean pressures. Comparison to the saturation curve indicates that the thermoacoustic effect significantly reduces the maximum temperature for a given pressure. In addition, it is notable that a heavier, more complex structured gas is associated with lower maximum temperature. (b)–(d) Stack temperature measurements at varying pressures compared to theoretical predictions calculated numerically. x is the stack length coordinate where $x = 0$ is the stack's cold end. Dots (from right to left) represent temperatures T3, T2, and T1, measured at distances of 5 mm, 15 mm, and 25 mm, respectively, from the stack's hot end. Solid lines represent theoretical predictions for a given pressure. Error bars indicate the range of measured values.

model results and our experimental measurements in all the considered gas mixtures, suggesting that the model captures the physics through which the use of heavier gases tends to decrease the system steady-state temperature. Relying on this encouraging comparison, the design of future systems may use this numerical tool to optimize the selection of a working gas mixture.

The apparent correlation between the acoustic power, numerically calculated based on the measured pressure amplitude (see the details in the supplementary material), and the experimentally evaluated mass transport along the stack is shown in Fig. 4. The dashed line is a linear regression fitted to the data, revealing a good qualitative agreement. A linear relation between the mass flux and acoustic intensity may be demonstrated theoretically by simplifying Eq. (1), using the expression derived by Weltsch *et al.*,[5] yielding

$$\dot{m} = \rho_m C_m \left(\mathrm{Re}\left[p_1 \tilde{u_1} \hat{G}\right] - D \frac{l_h}{R_g T_m^2} \frac{\mathrm{d}T_m}{\mathrm{d}x} \right), \tag{3}$$

where R_g is the universal gas constant, $\mathrm{d}C_m/\mathrm{d}x$ in Eq. (1) is expressed here in terms of the temperature gradient $\mathrm{d}T_m/\mathrm{d}x$ using the Clausius–Clapeyron relation, and $\hat{G}$ is a complex function, dependent upon the system geometry, the mean pressure p_m, resonant frequency ω, the temperature along the stack, and the gas mixture properties (see the supplementary material for the derivation). The first term in this expression is the "mass streaming" term, resulting from the interaction of the acoustic field with the concentration field. The second term represents molecular diffusion, with the concentration gradient converted to a temperature gradient using the Clausius–Clapeyron relation. As a first approximation, we treat $\hat{G}$ as a constant and neglect the contribution of molecular diffusion to the mass flux, resulting in

$$\dot{m} \approx 2\rho_m C_m \hat{G} I_A, \tag{4}$$

recalling that the acoustic intensity (power per unit cross-sectional area) is

$$I_A \equiv \frac{\omega}{2\pi} \int_0^{2\pi/\omega} p_1 u_1 \mathrm{d}t = \frac{1}{2} \mathrm{Re}[p_1 \tilde{u_1}]. \tag{5}$$

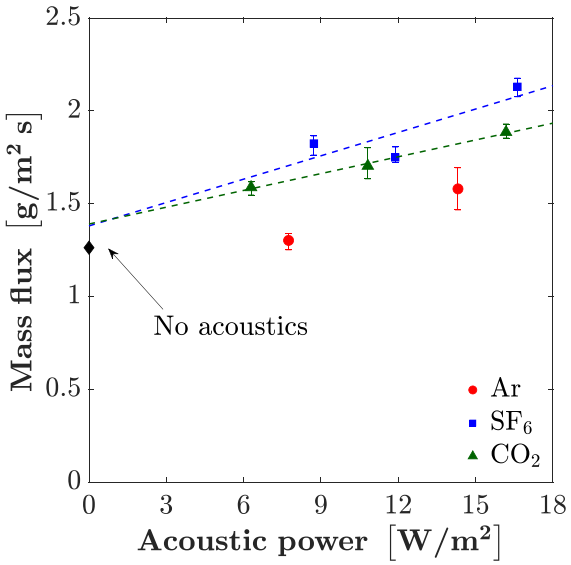

FIG. 4. Mass flux measurements vs the acoustic power flux (intensity), $I_A = \overline{p_1 u_1}$. Error bars indicate the range of measured values. The black diamond marks the averaged value of mass transport measurements taken at 1 bar in the damped mode ($\dot{m} = 1.32\,\mathrm{g\,m^{-2}\,s^{-1}}$). The dashed lines represent a linear fit of the CO_2 and SF_6 data, showing a good qualitative agreement with Eq. (4). These lines nearly intersect at $I_A = 0$, only slightly deviating from the measurement in the absence of acoustics.

The imperfect match between the experimental results and the linear lines in Fig. 4 is likely due to the assumptions made above, with which the linear relation in Eq. (4) was established theoretically. For example, the value of $\hat{G}$ varies for each gas mixture, meaning that each dataset would generally have a different slope as may be seen in Fig. 4. The qualitative trend, however, is well captured, suggesting that an increase in I_A should proportionally enhance the system mass transport.

To conclude, in the present study, we evaluated the heat and mass transport properties under the steady-state operation of a wet

thermoacoustic engine. We believe that the most remarkable observation is the evidence of the thermoacoustic field imposing a constraint on the maximal temperature of the liquid bulk, significantly lowering it compared to the saturation temperature for a given pressure. Further, the working gas characteristics were shown to play a key role in determining the value of the maximal temperature as well as other performance parameters such as the mass transfer rate and acoustic intensity. While fascinating in its own right, this effect might also be useful in thermal desalination processes, allowing facilities to employ low grade heat at lower temperatures. Further research is required in order to assess the applicability of the process in question to organic fluids, which might make it a candidate for distillation processes.

See the supplementary material for additional information on the experimental system and protocol, additional experimental data and full datasets, as well as the details of model derivation and numerical calculations.

This research was supported by Grant No. 216-11-024 from the Israel Ministry of Energy and Water. T.B. acknowledges the support from the Nancy and Stephen Grand Technion Energy Program (GTEP).

DATA AVAILABILITY

The data that support the findings of this study are available within this article and its supplementary material.

REFERENCES

[1]A. Elson, R. Tidball, and A. Hampson, *Waste Heat to Power Market Assessment* (Oakridge National Laboratory, U.S. Department of Energy, ICF International, Inc., 2015).
[2]A. Al-Karaghouli and L. Kazmerski, Renewable Sustainable Energy Rev. **24**, 343 (2013).
[3]A. S. Rattner and S. Garimella, "Energy harvesting, reuse and upgrade to reduce primary energy usage in the USA," Energy **36**, 6172 (2011).
[4]G. Swift, "Thermoacoustic engines," J. Acoust. Soc. Am. **84**, 1145 (1988).
[5]O. Weltsch, A. Offner, D. Liberzon, and G. Z. Ramon, "Adsorption mediated mass streaming," Phys. Rev. Lett. **118**, 244301 (2017).
[6]K. Tsuda and Y. Ueda, "Critical temperature of traveling and standing-wave thermoacoustic engines using a wet regenerator," Appl. Energy **196**, 62 (2017).
[7]A. Meir, A. Offner, and G. Z. Ramon, "Low-temperature energy conversion using a phase-change acoustic heat engine," Appl. Energy **231**, 372 (2018).
[8]Y. Blayer, N. Elkayam, and G. Z. Ramon, "Phase-dependence of sorption-induced mass streaming in an acoustic field," Appl. Phys. Lett. **115**, 033703 (2019).
[9]R. Yang, A. Meir, and G. Z. Ramon, "Theoretical performance characteristics of a travelling-wave phase-change thermoacoustic engine for low-grade heat recovery," Appl. Energy **261**, 114377 (2020).
[10]R. Raspet, W. V. Slaton, C. J. Hickey, and R. A. Hiller, "Theory of inert gas-condensing vapor thermoacoustics: Propagation equation," J. Acoust. Soc. Am. **112**, 1414–1422 (2002).
[11]B. Poling, J. O'Connell, and J. Prausnitz, *The Properties of Gases and Liquids*, 5th ed. (McGraw Hill, New York, 2001).
[12]C. Shen, Y. He, Y. Li, H. Ke, D. Zhang, and Y. Liu, "Performance of solar powered thermoacoustic engine at different tilted angles," Appl. Therm. Eng. **29**, 2745 (2009).
[13]A. Offner, R. Yang, D. Felman, N. Elkayam, Y. Agnon, and G. Z. Ramon, "Acoustic oscillations driven by boundary mass exchange," J. Fluid Mech. **866**, 316 (2019).